Optik xxx (2014) xxx–xxx

Contents lists available at ScienceDirect

Optik

journal homepage: www.elsevier.de/ijleo

Diffuse light transmission profiles obtained using *CW*: A comparative analysis with time resolved experiments

M. Waks Serra[a,b], N. Carbone[a,b], H. Di Rocco[a,b], H. García[a,b], D. Iriarte[a,b,*], J. Pomarico[a,b], H. Ranea-Sandoval[b]

[a] *CIFICEN, UNCPBA, CONICET, Pinto 399, B7000GHG Tandil, Argentina*
[b] *UNCPBA, CONICET, Argentina*

ARTICLE INFO

Article history:
Received 10 July 2013
Accepted 4 January 2014
Available online xxx

Keywords:
Turbid media
Transmittance
Inhomogeneities
Time resolved techniques

ABSTRACT

In this work, we investigate the *CW* transmitted light profiles when an inhomogeneity is immersed in highly scattering media slabs. These profiles show an interesting effect whenever the absorption coefficient, μ_a, of the inclusion happens to be higher than that of the bulk whereas its reduced scattering coefficient, μ_s', is lower than that of the surrounding medium. For this combination of optical properties, the transmitted light displays a peak of higher intensity at scan positions where the inclusion is located, producing a distinctive "*W*" profile. We have investigated this effect by analyzing the temporal windows of the distribution of times of flight at each scan position. In this way we found that the origin of the "*W*" profile is due to the contribution of the late photons. Experiments are compared with a theoretical model and with Monte Carlo simulations showing good agreement.

1. Introduction

The study of light propagation in turbid media such as biological tissue has achieved significant prominence. In the last decade, the use of red and near-infrared radiation (*NIR*) has been proposed as a tool for a possible noninvasive imaging modality to detect pathological processes leading to changes in optical properties of biological tissues [1–3]. The interest in this novel noninvasive tool relies on its capability to optically characterize the inhomogeneities and to obtain functional information of the tissues (composition, oxygenation, vascularization, etc.), thus complementing the established techniques used for localization.

The optical properties of interest to diagnose biological tissues are the absorption coefficient μ_a, and the reduced scattering coefficient defined as $\mu_s' = \mu_s(1-g)$, which is the inverse of the transport mean free path. The parameter μ_s is the scattering coefficient and g is the anisotropy factor.

However, the high number of scattering events in diffusive media, limits the clinical application of the methods based on image formation. To overcome this problem, several studies, both theoretical and experimental, have been performed in *CW* transillumination [4,5], in time domain [6,7], and in frequency domain [8–10], and proved to be valuable tools for improving contrast and spatial resolution in the imaging process [11,12].

From data reported by several authors [13–17], it can be concluded that for wavelengths in the *NIR* range, tumors are characterized by weaker scattering and significantly higher absorption with respect to the surrounding healthy tissue. On the contrary, accordingly with the measurements of Ghosh et al. [18], both optical parameters for malignant human breast tissue were found to be larger than the corresponding ones for the normal tissue. Other researchers have focused their attention on the study of the spatial resolution of the images in relation to the optical properties of tissue [19,20]. However, the problem of detecting inhomogeneities presents, in some particular cases, a combination of the optical properties that results in a difficult discrimination between absorbing and scattering inclusions. Grosenick et al. [21] carried out a detailed study in solid phantoms containing a cubical inhomogeneity which is more absorbing (factor 4) and less scattering (factor 0.3) than a background medium with optical properties similar to the human breast tissue showing "*W*"-like profiles. Similar structures have been reported by Danlewski [22] using Photon Density Waves (*PDW*) at modulation frequencies >250 MHz in experiments with absorbing inhomogeneities and have been explained by diffraction of *PDW* at them. Others similar dips have been observed and reported previously by diffuse photon density waves [23,24] Additionally, even though *CW* transillumination experiments exist for extracting the weakly scattered light (*WKL*)

* Corresponding author.
E-mail address: danielairi@gmail.com (D. Iriarte).

http://dx.doi.org/10.1016/j.ijleo.2014.02.003
0030-4026/

[5], time-integrated techniques based on a narrow time-window provides significant improvement in contrast, and spatial resolutions, when compared to *CW* techniques, as it is shown in [25].

In this work, we report a particular transmitted intensity profile in *CW* experiments when the inhomogeneity is more absorbing and less scattering than the background turbid medium, which is similar to that observed in Ref. [22]. This transmitted integrated intensity at positions where the inclusion is located shows a peak instead of the expected dip due to higher absorption, displaying a *W*-like structure [26]. To address this point, we compare the data obtained from experiments in *CW* to those using a Time Resolved (*TR*) technique. This last approach allows to separate photons that have experienced a relatively small number of scattering interactions, from late diffusive photons. We thus analyze the different behavior of early and late photons to separate the contributions of the fast and slow photons in the integrated intensity profiles, which in turns allows to explain the "*W*"-like structures observed in *CW* (i.e. $\omega = 0$) transillumination experiments.

Experimentally, we used jelly cylindrical inclusions immersed in liquid phantoms slabs, and the free surfaces of the phantoms were scanned along a line using a *NIR* laser in a *TR* transillumination mode. Analyzing the different deciles in the Distributions of Times of Flight (*DTOF*) of photons in the turbid media we give an interpretation about the origin of the "*W*" structure mentioned above.

The paper is organized as follows: In the following section we describe the problem in detail; in Section 3 the main theoretical considerations are explained; in Section 4 we present the different experimental aspects of the work, and in Section 5 the most important results are discussed. Finally, we summarize in Section 6 the most relevant conclusions.

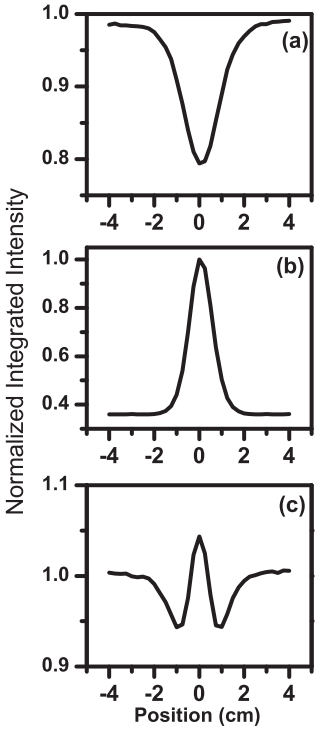

Fig. 1. Experimental transillumination profiles for agarose cylindrical inclusions embedded in a liquid phantom for different optical properties combinations: (a) $\mu_{aInc} > \mu_{aBck}$, (b) $\mu_{aInc} < \mu_{aBck}$, (c) $\mu_{aInc} \approx 2\mu_{aBck}$ and $\mu'_{sInc} < \mu'_{sBck}$. In all cases, the horizontal axis represents the source-detector pair position relative to center of the inclusion.

2. Description of the problem

As briefly stated in the Section 1, there are some experimental situations for which the interpretation of the results may be ambiguous. This can be the case for experiments in transillumination modality in which the integrated intensity is considered. In these set-ups (Fig. 1) the source and detector are facing each other defining the optical axis and they are scanned along a transversal direction of the surface of a turbid medium slab containing inhomogeneities. At each scan position, the transmitted diffuse intensity is registered, giving rise to a transillumination profile. When the inhomogeneities embedded are more absorbing than the background medium (that is, $\mu_{aInc} > \mu_{aBck}$), keeping all other parameters fixed, the expected transilluminance profiles are similar to the one shown in Fig. 1a. On the contrary, if the inclusion is less absorbing than the background, ($\mu_{aInc} < \mu_{aBck}$), the transillumination profile of Fig. 1b is expected. However, in some experimental situations in which $\mu_{aInc} > \mu_{aBck}$ and simultaneously $\mu'_{sInc} < \mu'_{sBck}$, the resulting profile shows a behavior similar as the one displayed in Fig. 1c. This figure presents an increase in the transmitted intensity when light goes through the absorbing inclusion, in apparent contradiction with the regular result of Fig. 1a.

Taking into account the above arguments, and considering that the special situation of Fig. 1c, we designed and carried out a series of controlled experiments to determine under which conditions it is possible to observe this kind of transilluminance "*W*"-like profile. In doing so, the inclusion was an absorbing cylinder made of a mixture of distilled water, milk, India ink and agarose, used as a jellying agent. It was immersed in a slab filled also with a water, milk and India Ink solution. Details about the experimental setup and phantom preparation are given in Section 4.

The transmittance profiles were compared to a theoretical model for turbid media with cylindrical inclusions, [10,27], which will be described thoroughly in the next section.

3. Theoretical considerations

In order to theoretically describe our results, we use here the expressions from the diffusion approximation (*DA*) of the radiative transfer equation (*RTE*). Closed theoretical solutions exist only for a few simple systems, such as homogeneous media (without inclusions) in infinite, semi-infinite and slab configurations [28]. There are also a number of solutions for the inhomogeneous problem containing a sphere [29] or an infinitely long cylinder [30] immersed in a infinite medium; the last situation has also been recently revised by some of the authors in [27]. For semi-infinite and slabs geometries, it is known that the solutions require to take into account a series of image sources charges adequately positioned.

The fundamental solution of the diffusion equation is the fluence in infinite media. For a point-like source in space and time, $S(\mathbf{r}, \mathbf{r}_s, t) = \delta(\mathbf{r} - \mathbf{r}_s)\delta(t)$, this solution reads:

$$\phi(r_{sd}, t) = \frac{z_0}{(4\pi Dvt)^{3/2}} \exp\left(-\frac{r_{sd}^2}{4Dvt} - \mu_a vt\right) \quad (1)$$

where $\mathbf{r}_s$ is the source position, r_{sd} is the distance between the source and detector, D is the diffusion coefficient ($D = 1/(3\mu'_s + \mu_a) \approx 1/3\mu'_s$ for DA), $v = c/n$ is the speed of light inside the diffusing medium and $z_0 = 1/\mu'_s$.

From this equation, the transmittance $T(r, t)$ [28] can be found. Besides, after time integration, the time independent transmittance $T(r)$ is obtained; this is the value measured using *CW* techniques.

If a sphere of optical parameters (μ'_{sInc}, μ_{aInc}) is embedded in a homogeneous medium with coefficients (μ'_{sBck}, μ_{aBck}), the total

Please cite this article in press as: M. Waks Serra, et al., Diffuse light transmission profiles obtained using *CW*: A comparative analysis with time resolved experiments, Optik - Int. J. Light Electron Opt. (2014), http://dx.doi.org/10.1016/j.ijleo.2014.02.003

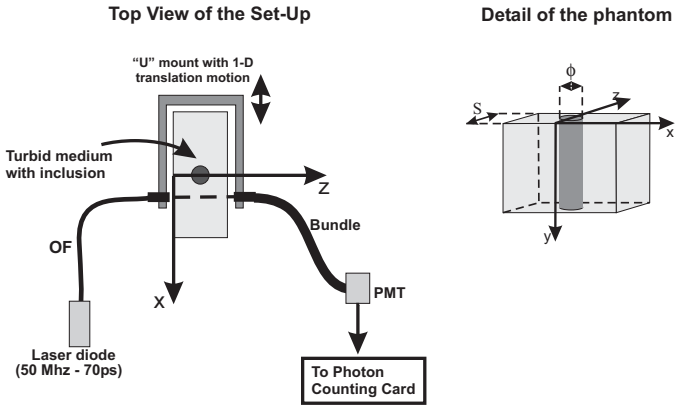

Fig. 2. Experimental set-up for the time-resolved transillumination experiments and schematic representation of the phantom.

fluence in steady state can be found as the sum of the source fluence, $\Phi_0(r)$, and the perturbation, $\Phi_{scatt}(\mathbf{r})$, as [29]

$$\Phi(\mathbf{r}) = \Phi_0(\mathbf{r}) + \Phi_{scatt}(\mathbf{r}) = \Phi_0(\mathbf{r}) + \sum_{m=0}^{\infty} B_m k_m(\kappa r) P_m(\cos\theta), \quad (2)$$

being k_m the modified Bessel functions of order m, and $\kappa = \sqrt{3\mu_s'\mu_a}$ the effective attenuation coefficient. The B_m coefficients are found by applying the adequate boundary conditions.

Analogously, when the inhomogeneity is a cylinder, following the same procedure as for the sphere, the solutions obtained are [27,30]

$$\Phi_{scatt}(\mathbf{r}_s, \mathbf{r}_d) = \int_0^{\infty} dp \left\{ B_0 k_0\left(\sqrt{p^2+\kappa_{out}^2}\rho_d\right) + 2\sum_{m=1}^{\infty} \cos(py_d)\cos(m\pi) k_m\left(\sqrt{p^2+\kappa_{out}^2}\rho_d\right) \right\}. \quad (3)$$

4. Experiments

All experiments were performed using the *TR* technique. This has the advantage that the desired *CW* information is obtained by time integration of the resulting *DTOF*'s while still preserving all information characteristic for time-domain analysis.

4.1. Phantoms preparation

Phantoms used in this work are build up from two components: (a) a liquid part which constitutes the background medium, and (b) a cylindrical inclusion of agarose. See Fig. 2.

The liquid part used was prepared by filling a fish tank of dimensions 24 cm × 24 cm × 3 cm with a solution of distilled water, milk, and 1:1000 diluted India Ink. Milk and India Ink proportions were conveniently varied for each individual experiment. The inclusions were made with a similar mixture of distilled water, milk and India Ink, in a block of dimension 16 cm × 24 cm × 3 cm, adding 2% of agarose to make it jellify. The optical properties of these inhomogeneities were measured using this block. The cylinders constituting the actual inclusions were extracted from it by cutting them out with the help of a plastic cylindrical hollow cutter, which was pushed into the block. The resulting inclusion was thus a cylinder of diameter $\phi_{Inc} = 1.3$ cm and length $l = 16$ cm. Note that this procedure requires good homogeneity in the optical properties of the block. They were thus measured at several positions and the cylinders were cut out from those regions presenting more uniformity.

4.2. Measurements of the optical properties

In the experiments presented in this work, previous measurement of optical properties of the two components of the phantom are mandatory. For determining the optical properties of both, the liquid and the jellyfied block, we used the time-resolved approach, by fitting the *DTOF*'s to the theoretical model developed for slabs in the work by Contini et al. [28].

The expression for the diffuse transmittance $T(s, \rho, t)$ per unit time and unit area, for a slab of reduced scattering coefficient μ_s' and absorption coefficient μ_a, results [28]:

$$T(s,\rho,t) = \frac{\exp(-\mu_a v t - (\rho^2/4Dvt))}{2(4\pi Dv)^{3/2} t^{5/2}} \times \sum_{m=-\infty}^{\infty} \begin{bmatrix} z_{1m}\exp\left(-\frac{z_{1m}^2}{4Dvt}\right) \\ -z_{2m}\exp\left(-\frac{z_{2m}^2}{4Dvt}\right) \end{bmatrix}, \quad (4)$$

where $z_{1m} = s(1-2m) - 4mz_e - z_0$, $z_{2m} = s(1-2m) - (4m-2)z_e + z_0$, and, for a refractive index $n = 1.42$, $z_e \approx 2.05/\mu_s'$ is the extrapolated distance where the diffuse intensity, $U(r)$ vanishes.

The measured *DTOF*'s, together with the corresponding Instrument Response Function (*IRF*) are given as inputs in a Levenberg–Marquardt routine, which in turn gives the set of optical parameters that minimizes errors.

4.3. Transilluminance controlled experiments

The experimental set up for the time-resolved transillumination experiments can be seen in Fig. 2. A diode laser emits 70 ps pulses at $\lambda = 785$ nm and at 50 MHz repetition rate, with an average power of 1.6 mW. The light pulses are injected into the turbid medium via a 400 μm diameter optical fiber emulating a point source. Photons are collected at the exit by an optical fiber bundle ($\phi = 4$ mm) facing the first one. Both fibers are scanned together using a rigid "U" device driven by a motorized linear translation stage with micrometer resolution (Zaber Technologies) along a 12 cm long line in 2.5 mm steps. At each position, the corresponding transmittance *DTOF*, was registered by sending the diffuse light exiting the phantom to a high sensitivity detector (*PMT*) in single-photon collection mode, connected to a Time-Correlated Single Photon Counting (*TCSPC*) electronics (*SPC* 130, Becker & Hickl GmbH, Germany) and displayed on a *PC* monitor.

The turbid medium used for this experiment was a fish tank of dimensions 24 cm × 24 cm and thickness $S = 3$ cm, initially filled with the solution explained above, in proportions 3:0.8:0.019 (distilled water: whole milk: diluted India Ink). The cylindrical inclusion, constructed as described above, was placed inside the tank at $z = 1.5$ cm depth, equidistant from the light input and output faces. Its horizontal position is taken as $x = 0$, and thus scanning is performed in the interval $-6\,\text{cm} \le x \le +6\,\text{cm}$.

Since varying the optical properties of the jellyfied cylinder is cumbersome, we vary the optical properties of the liquid background relative to those of the inclusion. We carried out then a series of transilluminance experiments, modifying the milk concentration of the liquid solution and keeping constant the ratio between the absorption coefficients of both, the background and the inclusion, around $\mu_{aInc} \gtrsim 2\mu_{aBck}$. The proportion of added milk at each experiment was 1.7% of the total volume of the solution, giving rise to increments in the reduced scattering coefficient of $\Delta\mu_{sBck}' \approx 0.7\,\text{cm}^{-1}$/step.

Please cite this article in press as: M. Waks Serra, et al., Diffuse light transmission profiles obtained using *CW*: A comparative analysis with time resolved experiments, Optik - Int. J. Light Electron Opt. (2014), http://dx.doi.org/10.1016/j.ijleo.2014.02.003

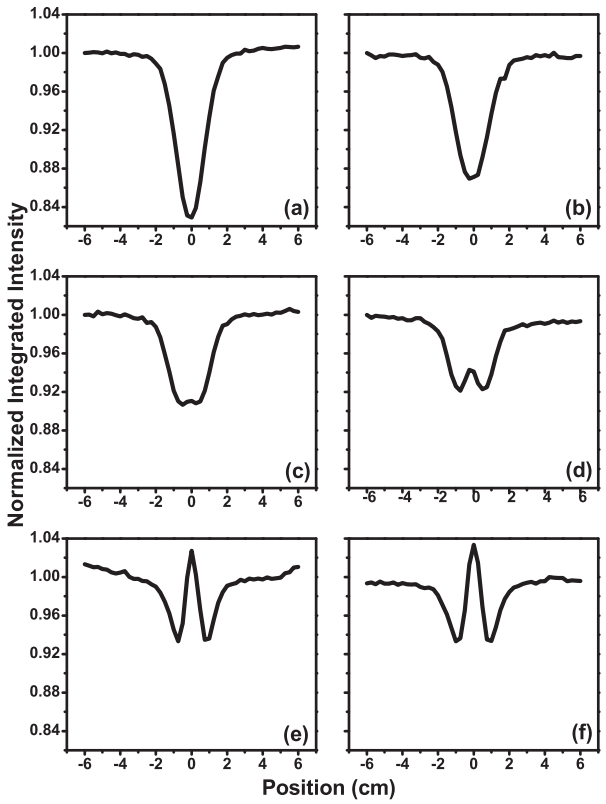

Fig. 3. Sequence of integrated intensity profiles of the *DTOF*'s (normalized to the transmitted intensity far from the inclusion) obtained at the different scan positions and for different concentrations of milk in the liquid solution. Optical properties used are listed in Table 1.

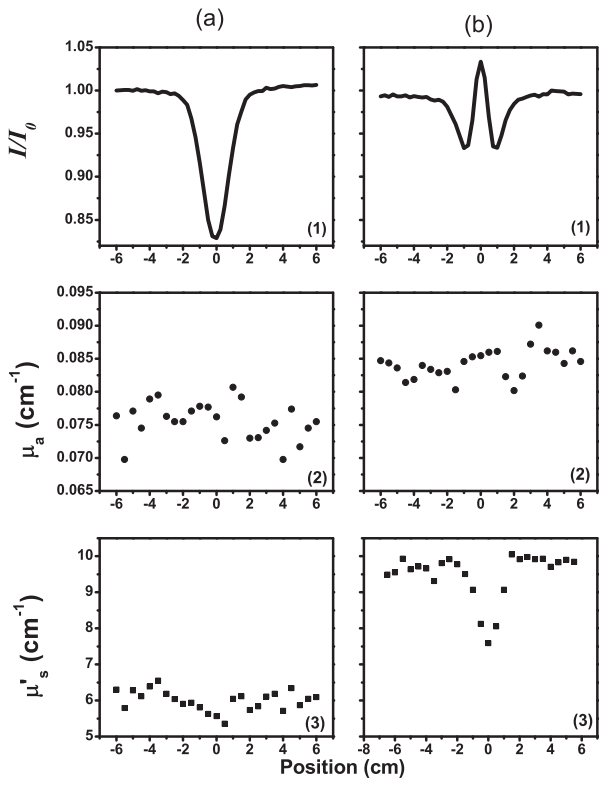

Fig. 4. Retrieved effective optical properties by fitting the *DTOF*'s at each horizontal scan position: (a1) and (b1) are the transillumination profiles given in Fig. 3a and f respectively. (a2) and (b2) represent the effective absorption coefficient and in (a3) and (b3) give the effective scattering coefficient. Note that from Figures (a2) and (a3) the profile in (a1) cannot be inferred. Similarly, from (b2) and (b3) the profile (b1) cannot be fully understood.

Table 1
Composition of the liquid part of the phantom and the resulting fitted optical properties corresponding to the experiments shown in Fig. 3.

Liquid part composition distilled water:whole milk:diluted India Ink	μ_{aBck} (cm^{-1})	μ'_{sBck} (cm^{-1})
3:0.8:0.019 (Fig. 3a)	0.0757 ± 0.0044	5.09 ± 0.3
3:0.9:0.0195 (Fig. 3b)	0.0826 ± 0.0015	6.15 ± 0.15
3:1:0.02 (Fig. 3c)	0.0838 ± 0.0015	6.93 ± 0.15
3:1.1:0.0205 (Fig. 3d)	0.0856 ± 0.0022	7.48 ± 0.18
3:1.2:0.021 (Fig. 3e)	0.0867 ± 0.0017	8.26 ± 0.3
3:1.3:0.0215 (Fig. 3f)	0.0889 ± 0.0013	9.01 ± 0.09

5. Results and discussion

The results of the experiments described above are shown in Fig. 3. Each curve in this figure represents the normalized integrated intensity of the *DTOF*'s obtained at the different scanned positions for different concentrations of milk in the liquid solution. The optical parameters of the cylinder were previously measured by fitting the *DTOF* to the model of Eq. (4) and they resulted to be $\mu_{aInc} = 0.12 \pm 0.02\,\text{cm}^{-1}$ and $\mu'_{sInc} = 5.12 \pm 0.7\,\text{cm}^{-1}$. They were kept unchanged for all situations depicted in Fig. 3. The optical properties of the background are listed in Table 1.

Fig. 3a, shows the transilluminance profile for the case $\mu_{aBck} = 0.0757\,\text{cm}^{-1}$ and $\mu'_{sBck} = 5.09\,\text{cm}^{-1}$. The absorbing nature of the inclusion results evident. Subsequent profiles, were obtained by adding more milk and the respective proportion of absorber as to keep constant the ratio μ_{aInc}/μ_{aBck}. Fig. 3b and c shows a similar behavior as Fig. 3a. The modulation is reduced due to the increasing scattering coefficient of the background. Fig. 3d–f shows a central peak, which becomes more and more prominent as μ'_{sBck} increases from $\mu'_{sBck} = 7.48\,\text{cm}^{-1}$ (Fig. 3d), to $\mu'_{sBck} = 9.01\,\text{cm}^{-1}$ (Fig. 3f). The occurrence of this peak makes the integrated intensity profiles to look as if there were two absorbing inclusions embedded in the liquid solution. Thus, this ambiguity in the interpretation in the profile arises due only to the lower reduced scattering coefficient of the inclusion relative to that of the background, even for the case of an absorbing inclusion.

In the following, we use the results shown in Fig. 3a and f for a deeper analysis of the situation involving the study of the optical properties obtained by two different approaches: the fitting of the *DTOF*'s using a Levenberg–Marquardt routine, and a statistical method based on dividing the *DTOF*'s in ten time-intervals, called *deciles*, as we shall clarify later.

5.1. Effective coefficients

In certain cases, in order to detect and characterize hidden objects inside a diffusive medium, the system is approximated as a homogeneous slab or as a homogeneous semi-infinite medium. This assumption drives the analysis to bring effective local values (background + inclusion) at those scan positions where the inclusion is present. In our geometry these positions are within the interval $-0.65\,\text{cm} \le x \le +0.65\,\text{cm}$, accordingly with the 1.3 cm of the cylinder diameter. We will call these effective local parameters $\langle \mu'_S \rangle$ and $\langle \mu_a \rangle$. This approximation has been already used by other authors specially in the cases involving multilayer analysis and photon density waves [21,31].

The results of fitting the *DTOF*'s using the homogeneous model of Eq. (4) for each scan position are shown in Fig. 4. Fig. 4a1 and b1 represents a duplicate of the transilluminance profiles shown in Fig. 3a and f, respectively. Fig. 4a2 and b2 are the results of the

evaluation of the effective local absorption coefficient for these special cases, and Fig. 4a3 and b3 shows the corresponding effective local reduced scattering coefficients.

An inspection of these parameters neither explains the appearance of the central dip in Fig. 4a1 nor the "*W*" profile in Fig. 4b1. In fact, for the case of the profile of Fig. 4a1, both, the local reduced scattering coefficient and the local absorption coefficient (Fig. 4a2 and a3) does not present any variations at the inclusion beyond the experimental fluctuations. In the case of Fig. 4b, only a reduction in the reduced scattering coefficient is observed (Fig. 4b3), which is compatible with an intensity rise at the centre but cannot account for the intensity drop at both sides of the peak.

Note that even a simplified and naïve calculation using the weighted average values of the optical properties, for example for the case of Fig. 4a2 at the position coincident with the centre of the inclusion ($x = 0$), gives (see Fig. 2):

$$\bar{\mu_a} = \frac{(S - \phi_{Inc})\mu_{aBck} + \phi_{Inc}\mu_{aI}}{S}.$$

Using in this last equation $S = 3$ cm, $\phi_{Inc} = 1.3$ cm, and the optical properties given in Table 1, we obtain:

$$\bar{\mu_a} \cong 0.094\,\text{cm}^{-1},$$

a value of the average absorption coefficient which is clearly different from the value of μ_a far from the inclusion ($\sim 0.075\,\text{cm}^{-1}$) and well beyond the experimental fluctuations. Thus, it only could explain the drop in the intensity transilluminance profile near the inclusion.

Similar results are obtained for the cases of Fig. 4a3, b2, and b3.

As a consequence, we conclude that using a homogeneous model to determine the effective optical properties of a turbid medium with an inclusion constitutes an oversimplification which bring erroneous values, at least for cases in which the optical properties of the background are not quite different from those of the inclusion.

5.2. Analysis of the origin of the "W" profiles

Similar "*W*"-like transillumination profiles as reported here have been observed before in frequency domain experiments and have been explained by diffraction [21,22] of strongly damped photon density waves (*PDW*) at inhomogeneities in otherwise homogeneous scattering media. However, the physical picture of *PDW* diffraction phenomena is not really helpful in case of *CW* experiments since for zero frequency there is no *PDW* at all, and hence no diffraction. Another possible approach to this problem is to study the number of photons present in different portions of the *DTOF* as we describe below.

It is a well established fact, that for a given *DTOF*, its rising edge (early photons) is more sensitive to changes in μ_s', while the behavior of its tail (late photons) is dominated by μ_a.

We have used this property to analyze changes in the optical parameters relative to a reference value, using the deciles of the *DTOF*'s. This method divides each *DTOF* in ten time - sections, each containing an equal number of photons, called "decile". A reference *DTOF* (far from the inclusion) is used to determine the time points t_j that define the deciles. As stated, the number of photons in the first decile ($t_0 \le t < t_1$) of the *DTOF* is more sensitive to changes in the reduced scattering coefficient, μ_s', while the eighth decile ($t_7 \le t < t_8$) follows the variations of the absorption coefficient, μ_a, of the medium.

We analyze here the temporal pulses for all cases presented in Fig. 3, using the statistical criteria of the deciles. Results for the first and eighth decile are shown in Figs. 5 and 6, respectively. From the analysis of the first decile (Fig. 5) an increment of its value is noticed at positions where the input beam coincides with those where the

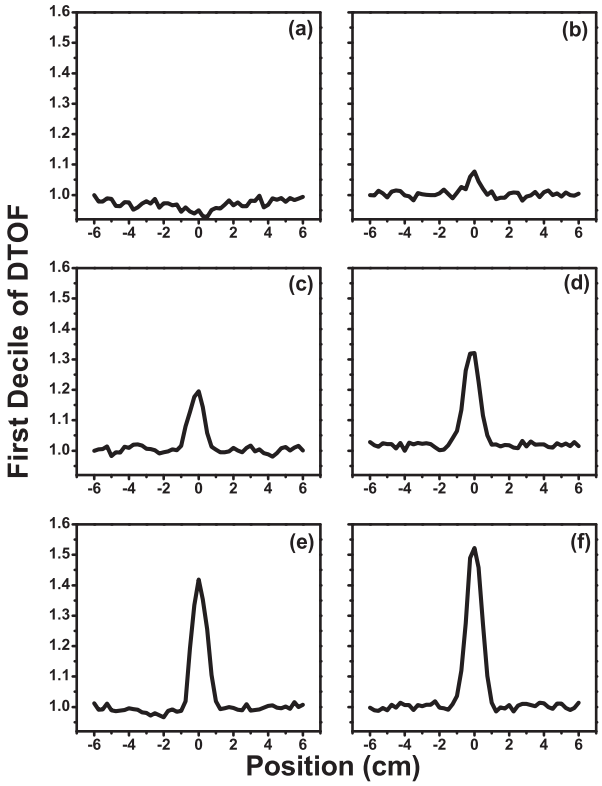

Fig. 5. Analysis of the sequential experiments of Fig. 3 displaying the number of photons in the first decile of the corresponding *DTOF* at each horizontal scan position. Fig. 5a–f correspond to Fig. 3a–f, respectively. Note the increment in the number of photons at the inclusion as the ratio μ'_{sInc}/μ'_{sBkg} decreases. Each curve is normalized to its value at positions far from the inclusion.

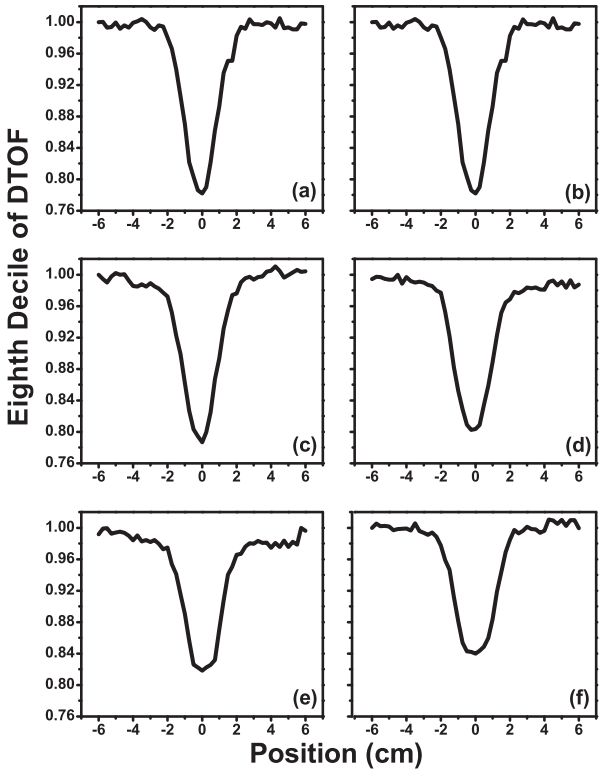

Fig. 6. Analysis of the sequential experiments of Fig. 3 displaying the number of photons in the eighth decile of the corresponding *DTOF* at each horizontal scan position. Fig. 6a–f correspond to Fig. 3a–f, respectively. Note the reduced number of photons at the inclusion due to the ratio $(\mu_{aInc}/\mu_{aBkg}) > 1$. Each curve is normalized to its value at positions far from the inclusion.

Please cite this article in press as: M. Waks Serra, et al., Diffuse light transmission profiles obtained using *CW*: A comparative analysis with time resolved experiments, Optik - Int. J. Light Electron Opt. (2014), http://dx.doi.org/10.1016/j.ijleo.2014.02.003

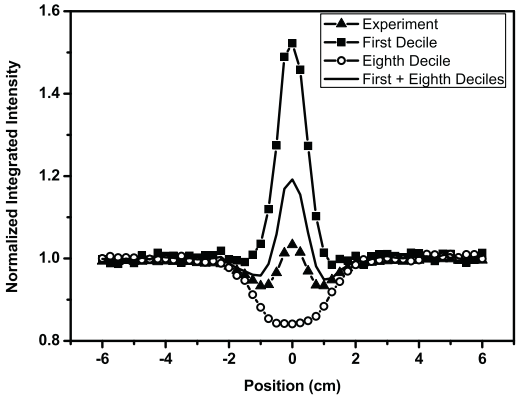

Fig. 7. Interpretation of the experimental profile in terms of the deciles. The triangles represent the experimental profile corresponding to Fig. 3f, squares and open circles represent the first and eighth decile of the *DTOF*'s for this experiment, respectively. The solid line shows the sum of the first decile and the eighth decile.

cylindrical inclusion is present, in particular in Fig. 5c–f. This means that a greater number of early photons is present in the resulting *DTOF*'s, which is consistent with a decrease in the average local scattering coefficient. Moreover, the width of this first decile curve, measured at the baseline, coincides very well with the diameter of the inclusion. In other words, in some cases (Fig. 5c–f) it is possible to identify the presence of the (less scattering) inclusion following the behavior of the population of the first decile.

In Fig. 6, the eighth decile in turns, displays a decrease in the vicinity of the inclusion. This drop clearly means that less photons are present in the *DTOF*'s curves and could be explained by stating that an increase in the average local absorption coefficient has occurred, in agreement with the optical properties measured for the inclusion.

This analysis shows that using the deciles approach is more sensitive to changes in local optical properties since, as it has been shown in Fig. 4, fitting the *DTOF*'s not necessarily indicates an increment in the average absorption coefficient when the inclusion lies between the optodes.

With the help of Fig. 7 it is readily seen how the "*W*" structure originates. In fact, in Fig. 7 we show (squares), that the first decile contributes to a build up at the central prominent portion in the "*W*". In this figure the open circles, indicate that the values of the eighth decile account for the dip in the complete transilluminance profile. From these last two it is straightforward to notice that adding up both contributions, the "*W*" profile arises, a result that is shown in Fig. 7 as the solid line. For completeness, the experimental profile is also shown (triangles) corresponding to Fig. 3f.

In addition, we describe here the results of comparing Fig. 3 with the corresponding profiles obtained using the theoretical model presented in Section 3 and Monte Carlo (*MC*) simulations.

In Fig. 8a and b we reproduce the profiles shown in Fig. 3a and f, respectively, together with the corresponding theoretical and *MC* ones. They were calculated with the optical properties measured for both, the liquid part of the phantom and the inclusion itself, as described in Section 4.2, choosing the best combination within the experimental error (estimated to be 10%). For the case of Fig. 8a the optical properties used for the theoretical and MC calculations were $\mu'_{sInc} = 5\,\mathrm{cm}^{-1}$, $\mu'_{sBck} = 5.1\,\mathrm{cm}^{-1}$, $\mu_{aBck} = 0.075\,\mathrm{cm}^{-1}$, $\mu_{aInc} = 0.132$ and for Fig. 8b the resulted $\mu'_{sInc} = 5\,\mathrm{cm}^{-1}$, $\mu'_{sBck} = 8.2\,\mathrm{cm}^{-1}$, $\mu_{aBck} = 0.083\,\mathrm{cm}^{-1}$, $\mu_{aInc} = 0.132$. It can be seen that, even though the matching is not exact, in both cases the most important characteristics of the profile are correctly reproduced, that is, Fig. 8a shows no "*W*" profile while Fig. 8b does it.

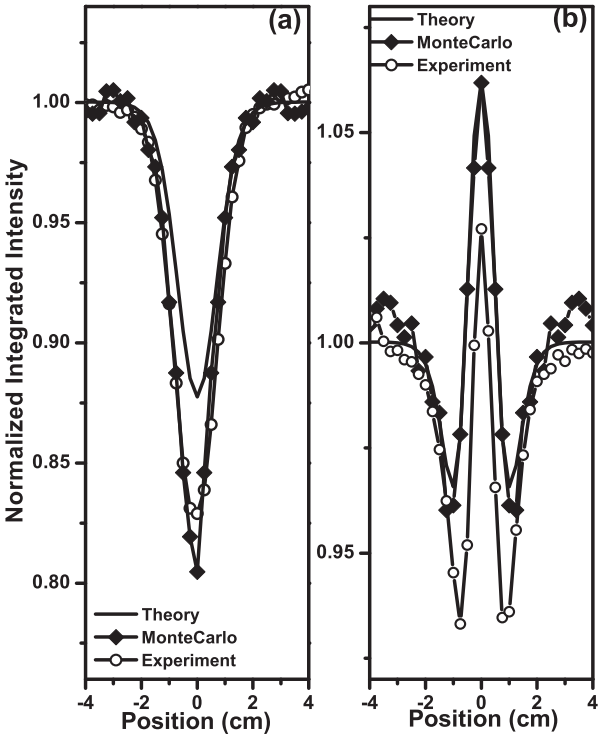

Fig. 8. Comparison of the experiment with Theory and Monte Carlo Simulations. (a) The experimental profile of Fig. 3a (hollow circles) compared to the results obtained by *MC* (diamond) and to the theory (solid line) if the measured optical properties of both, background and inclusion, are used. (b) Idem (a) but using the experimental profile as Fig. 3e with the optical properties shown in Table 1.

6. Conclusions

In this work we have investigated the behavior of the transilluminance profiles when absorbing inclusions are present in turbid media slabs. This was motivated by the fact that, in some cases, the transilluminance profiles show an increment in the integrated transmitted intensity, at positions where the inclusion is present, instead of a reduction of this intensity as could be expected for an absorbing inclusion.

We have demonstrated that this apparent contradiction can be explained if the reduced scattering coefficient of the inclusion is also considered. In fact, if the reduced scattering of the inhomogeneity is sufficiently smaller than that of the background, it can compensate, or even reverse, the effect of increased local absorption. Consequently, an intensity peak is observed at the center of the inclusion (Fig. 3d–f).

Moreover, from the decile analysis we conclude that this method allows to understand the origin of "*W*" profile. We showed that this special transilluminance profile is not observed by taking into account only the early photons, but it clearly arises if we consider the contribution of the late photons, together with the early ones.

Additionally, the decile method has proven to be more robust for the qualitative determination of the fluctuations in the optical properties with respect to some reference values, providing a helpful tool for a quick analysis in transilluminance scanning experiments. On the contrary, fitting of the *DTOF*'s to the homogeneous slab model fails to detect these fluctuations, since the model is oversimplified.

Acknowledgements

Authors are grateful to Proff. Rainer Macdonald for suggestions and helpful discussions about this work.

Please cite this article in press as: M. Waks Serra, et al., Diffuse light transmission profiles obtained using *CW*: A comparative analysis with time resolved experiments, Optik - Int. J. Light Electron Opt. (2014), http://dx.doi.org/10.1016/j.ijleo.2014.02.003

This paper is financially supported by the National Council of Science and Technology (CONICET), PIP 2010-2012, No. 384, ANPCyT, PICT 2008 No. 0570, Argentina.

References

[1] S. Andersson-Engels, R. Berg, O. Jarlman, S. Svanberg, Time-resolved imaging through a highly scattering medium, Opt. Lett. 15 (1990) 1179–1181.
[2] S. Andersson-Engels, R. Berg, S. Svanberg, Effects of optical constants on time-gated transillumination of tissue and tissue-like media, J. Photochem. Photobiol. B 16 (1992) 155–167.
[3] T. Vo-Dinh (Ed.), Biomedical Photonics Handbook, CRC Press, Boca Raton, 2003, see specially Chapters 2, 3, 4, 21 and 22 and references therein.
[4] K. Takagi, Y. Kato, K. Shimizu, Extraction of near-axis scattered light for transillumination imaging, Appl. Opt. 48 (2009) D36–D44.
[5] K. Takagi, H. Kakinuma, Y. Kato, K. Shimizu, CW transillumination imaging by extracting weakly scattered light from strongly diffused light, Opt. Express 17 (10) (2009) 8332–8342.
[6] M.S. Patterson, B. Chance, B.C. Wilson, Time-resolved reflectance and transmittance for the noninvasive measurement of tissue optical properties, Appl. Opt. 28 (1989) 2331–2336.
[7] J.C. Hebden, Imaging through scattering media using characteristics of the temporal distribution of transmitted laser pulses, Opt. Laser Technol. 27 (1995) 263–268.
[8] M.A. O'Leary, D.A. Boas, B. Chance, A.G. Yodh, Experimental images of heterogeneous turbid media by frequency-domain diffusing photon tomography, Opt. Lett. 20 (1995) 426–428.
[9] L.O. Svaasand, B.J. Tromberg, R.C. Haskell, T. Tsay, M.W. Berns, Tissue characterization and imaging using photon density waves, Opt. Eng. 32 (1993) 258–266.
[10] J. Fishkin, E. Gratton, Propagation of photon density waves in strongly scattering media containing an absorbing semi-infinite plane bounded by straight edge, J. Opt. Soc. Am. A 10 (1993) 127–140.
[11] R. Cubeddu, A. Pifferi, P. Taroni, A. Torricelli, G. Valentini, Time-resolved imaging on a realistic tissue phantom: μ_s' and μ_a images versus time-integrated images, Appl. Opt. 35 (22) (1996) 4533–4540.
[12] R. Cubeddu, A. Pifferi, P. Taroni, A. Torricelli, G. Valentini, Imaging with diffusing light: an experimental study of the effect of background optical properties, Appl. Opt. 37 (16) (1998) 3564–3573.
[13] D. Grosenick, K.T. Moesta, H. Wabnitz, J. Mucke, C. Stroszczynski, R. Macdonald, P.M. Schlag, H. Rinneberg, Time-domain optical mammography: initial clinical results on detection and characterization of breast tumors, Appl. Opt. 42 (2003) 3170–3186.
[14] D. Grosenick, H. Wabnitz, K.T. Moesta, J. Mucke, P.M. Schlag, H. Rinneberg, Time-domain scanning optical mammography: II. Optical properties and tissue parameters of 87 carcinomas, Phys. Med. Biol. 50 (2005) 2451–2468.
[15] T. Durduran, R. Choe, J.P. Culver, L. Zubkov, M.J. Holboke, J. Giammarco, B. Chance, A.G. Yodh, Bulk opticalproperties of healthy female breast tissue, Phys. Med. Biol. 47 (2002) 2847–2861.
[16] L. Spinelli, A. Torricelli, A. Pifferi, P. Taroni, G.M. Danesini, R. Cubeddu, Bulk optical properties and tissue components in the female breast from multiwavelength time-resolved optical mammography, J. Biomed. Opt. 9 (2004) 1137–1142.
[17] L. Steven, Jacques, Optical properties of biological tissues: a review, Phys. Med. Biol. 58 (2013) R37–R61.
[18] N. Ghosh, S.K. Mohanty, S.K. Majumder, P.K. Gupta, Measurement of optical transport properties of normal and malignant human breast tissue, Appl. Opt. 40 (2001) 176–184.
[19] G. Mitic, J. Kölzer, J. Otto, E. Piles, G. Sölkner, W. Zinth, Time-gated transillumination of biological tissues and tissue-like phantoms, Appl. Opt. 33 (1994) 6699–6710.
[20] J.C. Hebden, S.R. Arridge, D.T. Delpy, Optical imaging in medicine. I. Experimental techniques, Phys. Med. Biol. 42 (1997) 825–840.
[21] D. Grosenick, H. Wabnitz, H. Rinneberg, Time-resolved imaging of solid phantoms for optical mammography, Appl. Opt. 36 (1) (1997) 221–231.
[22] H. Danlewski, Physikalische Grundlagen der zeitaufgelösten optischen Mammographie, einschliesslich Anwendungen, Dissertation Frei Universität Berlin, 1998.
[23] S.A. Walker, D.A. Boas, E. Gratton, Photon density waves scattered from cylindrical inhomogeneities: theory and experiments, Appl. Opt. 37 (10) (1998) 1935–1944.
[24] J. Ripoll, M. Nieto-Vesperinas, R. Carminati, Spatial resolution of diffuse photon density waves, J. Opt. Soc. Am. A 16 (6) (1999).
[25] J. Hebden, A.H. Gandjbakhche, Estimating spatial resolution for optical transillumination imaging, Med. Phys. 22 (8) (1995) 1271–1272.
[26] N.A. Carbone, H.O. Di Rocco, D.I. Iriarte, J.A. Pomarico, H.F. Ranea-Sandoval, P. Pardini, M.V. Waks-Serra, Study of inhomogeneities in turbid media: experimental and numerical results, in: Proc. SPIE 8011, 22nd Congress of the International Commission for Optics: Light for the Development of the World, 80118P, 2011, http://dx.doi.org/10.1117/12.902166.
[27] H.O. Di Rocco, M. Lester, D.I. Iriarte, J. Pomarico, H.F. Ranea-Sandoval, CW laser transilluminance in turbid media with cylindrical inclusions, Optik 122 (2011) 577–581.
[28] D. Contini, F. Martelli, G. Zaccanti, Photon migration through a turbid slab described by a model based on diffusion approximation. I. Theory, Appl. Opt. 36 (19) (1997) 4587–4599.
[29] X.D. Zhu, S.-p. Wei, S.C. Feng, B. Chance, Analysis of a diffuse-photon-density wave in multiple-scattering media in the presence of a small spherical object, J. Opt. Soc. Am. A 23 (3) (1996) 494–499.
[30] A. Walker, D.A. Boas, E. Gratton, Photon density waves scattered form cylindrical inhomogeneities: theory and experiments, Appl. Opt. 37 (1997) 1935–1944.
[31] J. Ripoll Lorenzo, Light diffusion in turbid media with biomedical application, doctoral thesis presented in the Department of Condensed Matter Physics of the Science Faculty of the Universidad Autónoma de Madrid, Madrid, 2000.

Please cite this article in press as: M. Waks Serra, et al., Diffuse light transmission profiles obtained using *CW*: A comparative analysis with time resolved experiments, Optik - Int. J. Light Electron Opt. (2014), http://dx.doi.org/10.1016/j.ijleo.2014.02.003